Separation and Purification Technology 211 (2019) 151–161

Contents lists available at ScienceDirect

Separation and Purification Technology

journal homepage: www.elsevier.com/locate/seppur

Submerged vacuum membrane distillation crystallization (S-VMDC) with turbulent intensification for the concentration of NaCl solution

Tong Zou[a,b], Guodong Kang[a,*], Meiqing Zhou[a], Meng Li[a], Yiming Cao[a,*]

[a] Dalian National Laboratory for Clean Energy (DNL), Dalian Institute of Chemical Physics, Chinese Academy of Sciences, Dalian 116023, China
[b] University of Chinese Academy of Sciences, Beijing 100049, China

ARTICLE INFO

Keywords:
Submerged vacuum distillation
Crystallization
Turbulent intensification
Stirring
Micro-porous aeration

ABSTRACT

The feasibility of simultaneous pure water production and salt crystal recovery from highly concentration NaCl solution was evaluated by utilizing a submerged vacuum membrane distillation crystallization (S-VMDC) system with different turbulent intensification modes. The effect of intensification mode including stirring and aeration on membrane distillation performance and crystallization behavior was investigated systematically. An iterative method was used to evaluate the heat transfer enhancement effect. The results indicated that both stirring and aeration had positive influence on permeate flux due to the improvement of heat transfer and weakening of polarization phenomenon in boundary layer. The dominated crystallization behavior converted from surface crystallization to bulk crystallization with the help of turbulent intensification, which in turn increased the limiting concentration of the feed solution. The size and distribution of crystallized product could be regulated by selecting an optimal intensification mode. With the combined effect of stirring rate at 1350 rpm and aeration rate at 0.20 m^3/h, 31.85% NaCl crystals with relative desirable size distribution could be recovered from bulk solution. This study provided an alternative perspective to understand the enhancement effect of turbulent intensification strategy in S-VMDC process for concentrating saturation solution in both qualitative and quantitative ways.

1. Introduction

Membrane distillation (MD) is one of the non-isothermal separation processes known since 1963 and still needs to be developed to achieve industrial implementation [1]. The driving force in this separation process is the vapour pressure difference between two sides of hydrophobic membrane pores. For the feed solution containing non-volatile components, only vapour molecules can diffuse through the porous membrane to the permeate side. Therefore, theoretically complete separation takes place and preparation of high-purity water comes true [2]. One of the most excellent advantages of MD over reverse osmosis (RO) is that it shows great potential in the field of disposal of highly concentrated brines [3–5] without the influence of osmotic pressure gradient. Moreover, when MD combined with a crystallizer, pure water production and valuable salts recovery can be achieved simultaneously to realize the zero liquid discharge (ZLD) [6].

In conventional membrane distillation crystallization (MDC) process, the feed solution is concentrated to saturated or supersaturated condition through the MD and crystallized products are formed in an external crystallizer [7]. It is obvious that the operation in MDC is more challenging compared to MD since it is applied for the treatment of saturated solutions [8]. The effect of temperature and concentration polarization in highly concentrated solutions not only diminish the transmembrane driving force, but also facilitate the nucleation of salts near the membrane surface or in the membrane pores [9], which is known as crystallization fouling [10]. For example, Creusen et al. observed the blooming effect with both PTFE and PES membrane when treated a concentrated single salt solution of $CaCO_3$ or NaCl [11]. Chung et al. [8] studied the effect of feed temperature on polarization during simultaneous membrane distillation-crystallization process. To weaken the negative effect of polarization phenomenon, several attempts have been suggested including increasing flow velocity [12], introducing gas bubbling [13–15], designing new modules with baffles or spacers and modifying the geometry of hollow fibers [16]. Accompany with the heat transfer enhancement strategies mentioned above, the working mechanisms of these strategies were also explored based on the quantitative calculation of heat-transfer coefficients from the empirical model using Nusselt (*Nu*) and Sherwood (*Sh*) numbers [14,15]. The major limitation of this process is the heat loss caused by feed reheating and recirculation [17,18]. In addition, the risk of

* Corresponding authors.
E-mail addresses: kangguod@dicp.ac.cn (G. Kang), ymcao@dicp.ac.cn (Y. Cao).

https://doi.org/10.1016/j.seppur.2018.09.072
Received 21 June 2018; Received in revised form 17 September 2018; Accepted 25 September 2018
Available online 26 September 2018
1383-5866/ © 2018 Elsevier B.V. All rights reserved.

Nomenclature

A	effective area of membrane outer surface (m^2)
ΔH	latent heat of water vapour ($kJ\,kg^{-1}$)
h_f	heat transfer coefficient ($W\,m^2\,K^{-1}$)
J	permeate flux ($kg\,m^2\,h^{-1}$)
K_m	membrane distillation coefficient ($kg\,m^{-2}\,s^{-1}\,Pa^{-1}$)
M	molecular weight of water ($kg\,mol^{-1}$)
m	the weight of permeate (kg)
P^0	the pure water vapour pressure (Pa)
P_{fm}	the water vapor pressure at membrane surface (Pa)
P_v	pressure at the vacuum side (Pa)
R	universal gas constant ($J\,mol\,K^{-1}$)
T_f	temperature of solution in the feed bulk (K)
T_{fm}	temperature of solution at membrane surface (K)
T_v	equilibrium temperature corresponds to the pressure on permeate side (K)
TPC	temperature polarization coefficient
t	operation time (h)
r	mean pore size of membrane (m)
ε	membrane porosity
ε_e	membrane effective porosity
σ	membrane thickness (m)
τ	membrane turtuosity
ρ_f	the density of PTFE hollow fiber membrane (g/cm^3)
ρ_p	the density of PTFE polymer (g/cm^3)
x	mole fraction of NaCl in solution

blockage increases and the maintaining and cleaning are relatively difficult in conventional membrane module due to the relatively narrow flow channel of feed solution.

Recently, a novel submerged MD (SMD) configuration has been explored as an alternative to conventional MD and the feasibility was proved in a few studies [18,19]. When combined SMD with crystallization process (S-MDC), a membrane module without housing is submerged in a feed tank which serves as a crystallizer as well [17]. In this process, the need for feed reheating and recirculation is eliminated by the integration of MD and crystallization. Therefore, the energy consumption can be potentially minimized. Furthermore, the open configuration of the membrane module effectively prevents the blockage of flow channel and the blooming effect, making the maintenance and cleaning much easier. However, as the feed solution is stagnant during the S-MDC process, mass and heat transfer in boundary layer is relatively poor compared with the conventional cross-flow MDC. Intensification strategies such as transverse vibration [19], periodic air-backwash [20,21], aeration [17] and stirring [22] have been applied to improve the heat and mass transfer in boundary layer and avoid or reduce surface crystallization. But in most previously published work, the effect of these intensification strategies on heat transfer during S-MDC process still stayed on the qualitative description rather than quantitative analysis. In addition, there has been lack of systematically research about the effect of the turbulent intensification on both MD performance and crystallization behavior in submerged MDC process, especially when concentrating high salinity solution to saturation condition.

In this study, a self-made open "U-shaped" PTFE hollow fiber module without housing was directly immersed in a 100 g/L NaCl solution. A lab-scale submerged vacuum membrane distillation crystallization (S-VMDC) system was explored to produce pure water and desirable crystallized products simultaneously. The purpose of employing VMD was to minimize the energy consumption since heat conducted by membrane can be reduced by the presence of vacuum pressure. Two kinds of simple turbulent intensification techniques including stirring and micro-porous aeration were utilized to enhance the performance of S-VMDC. The effect of different turbulent intensification modes on the MD performance and crystallization behavior was investigated systemically. Furthermore, quantitative analysis of heat transfer coefficient (h_f) and temperature polarization coefficient (TPC) during S-VMDC process was evaluated by an iterative method based on the mass and heat transfer model of VMD.

2. Theory

In VMD, the driving force is maintained by applying a continuous vacuum at the permeate side. Once the vacuum pressure is applied, the partial pressure of non-condensable gases in the air such as N_2 and O_2 becomes very small compared with the water vapor molecules inside the membrane pores [23]. As a result, the resistance of these non-condensable gases to the mass transfer inside membrane pores is negligible and a linear relationship between the permeate flux (J) and the transmembrane water vapour pressure difference is established as Eq. (1) [24]:

$$J = k_m(P_{fm} - P_v) \tag{1}$$

where K_m is called VMD coefficient, P_{fm} is the water vapour pressure on membrane surface at T_{fm} and P_v is the pressure in the vacuum side. T_{fm} is the temperature of feed solution on the membrane surface.

As the mean free path of the water vapour is much larger than the pore size of the membrane used in this study, only Knudsen diffusion is considered during the mass transfer in this process [4]. Thus, the MD coefficient k_m can be written as Eq. (2):

$$k_m = 1.064\frac{r\varepsilon}{\tau\delta}\sqrt{\frac{M}{RT_{fm}}} \tag{2}$$

where r, ε, τ, σ is the mean pore size, porosity, membrane thickness and tortuosity, respectively. M is the molecular weight of water and R is the gas constant.

The pure water vapour pressure is given by the Antoine's equation [25]:

$$P^0 = \exp\left(23.1964 - \frac{3816.44}{T_{fm} - 46.13}\right) \tag{3}$$

The vapour pressure of the feed containing NaCl is given by Eq. (4) [5]:

$$P_{fm} = P^0(1-x)(1-0.5x-10x^2) \tag{4}$$

where x is the mole fraction of NaCl in feed solution.

In VMD, the heat transfer within the membrane is due to the latent heat accompanying vapour flux, while the boundary layer resistance on the permeate side and the contribution of the thermal conduction through membrane has been neglected [23]. In this case, the thermal balance on the feed side of the membrane can be written as Eq. (5) [26]:

$$J \cdot \Delta H = h_f(T_f - T_{fm}) \tag{5}$$

where hf is the heat transfer coefficient from the feed bulk to the membrane surface. Tf and Tfm is the temperature of the solution in the feed bulk and on the membrane surface, respectively. ΔH is the latent heat of water vapour at temperature of Tfm, which can be calculated using Eq. (6) [15]

$$\Delta H = 2258.4 + 2.47(373 - T_{fm}) \tag{6}$$

The temperature polarization coefficient (TPC) can be calculated according to its definition as Eq. (7) [27,28]:

$$TPC = \frac{T_{fm} - T_v}{T_f - T_v} \tag{7}$$

When TPC approaches a value of 1, it signifies the h_f approaches infinity for the case where heat transfer resistance in the liquid feed is negligible. While when TPC approaches to a value of 0, it implies that the flux is limited by heat transfer resistance [29].

3. Experimental

3.1. Membrane used in S-VMDC

3.1.1. Preparation of PTFE hollow fiber membrane

As a crystalline polymer, PTFE owns its superior properties such as hydrophobicity, thermal stability, chemical resistance and mechanical strength [30,31]. It is considered to be an ideal material especially for MD process compared with PVDF and PP [30,32,33]. The PTFE hollow fiber membrane used in this study was self-made with an approach which involved mixing and aging, billet preforming, paste extrusion, stretching and sintering. The detailed information about its preparation method was shown in our previous work [34,35].

3.1.2. Membrane porosity

The porosity of PTFE membrane was determined by the density measurement according to the Eq. (8) [36]

$$\varepsilon(\%) = \left(1 - \frac{\rho_f}{\rho_p}\right) \times 100 \tag{8}$$

where ρ_f is the density of a porous PTFE hollow fiber, and ρ_p is the density of the polymer. ρ_f was calculated by Eq. (9).

$$\rho_f = \frac{w}{\pi L(R^2 - r^2)} \tag{9}$$

W is the weight of the hollow fiber, L is the fiber length, R and r are the outer and inner radius, respectively.

3.1.3. Tortuosity

The tortuosity of the PTFE membrane was measured by the gas permeation test. This method was to measure the gas flow rate through a dry porous membrane at different transmembrane pressures. The detailed method was provided elsewhere [37]. The tortuosity was calculated according to the Eq. (10)

$$\tau = \frac{\varepsilon}{\sigma \varepsilon_e} \tag{10}$$

where ε_e is the effective porosity derived from gas permeation test, σ is the membrane thickness.

3.1.4. Mean pore size

The mean pore size of the PTFE membrane was measured by a liquid–liquid displacement method. The membrane was wetted by isobutanol first and then replaced with water by increasing the applied pressure stepwise. The detailed method is supplied elsewhere [38].

3.1.5. Liquid entry pressure (LEP_w)

The LEP value was obtained at room temperature. A PTFE hollow fiber having a length about 25 cm were assembled with epoxy resin and then connected to the outlet of a pressurized water tank. The applied pressure was increased stepwise by means of a pressure valve. The pressure at which a flow was observed at the external surface of the membrane is the LEP_w [39].

3.2. Membrane module used in S-VMDC

Six PTFE hollow fiber membranes with effective length of 50 cm were folded together to fabricate a simplified "U-shaped" membrane module, sealed with an epoxy resin at one end. The membrane module was reused by simple water cleaning. It was confirmed that the performance of this module was relatively stable either in reuse or continuous operation during our experiment. The parameter of the membrane module as well as the membrane properties obtained experimentally in Section 3.1 was listed in Table 1.

Table 1
The parameters of PTFE membrane and membrane module.

PTFE hollow fiber membrane	
Outer diameter (mm)	1.7
Inner diameter (mm)	0.8
Wall thickness (μm)	450
Porosity (%)	41.0
Tortuosity	2.6
Mean pore size (μm)	0.186
LEP_W (bar)	3.1
Membrane module for VMDC	
Effective length of membranes (cm)	50
No. of PTFE hollow fibers	6
Effective area of membranes (m^2)	0.016

3.3. Feed solution

The pure water flux J_0 was evaluated with deionized (DI) water as feed solution. The S-VMDC performance in concentration process was investigated by using 100 g/L NaCl solution. The NaCl solution was prepared by dissolving a certain amount of NaCl in deionized water. NaCl was purchased from Tianjin Kemiou Chemical Reagent Company and used without further purification.

3.4. Submerged vacuum membrane distillation crystallization (S-VMDC)

The experimental set-up of the S-VMDC used in this study is illustrated in Fig. 1. 100 g/L NaCl solution with the initial volume of 1000 mL was used as the feed solution. The "U-shaped" PTFE hollow fiber membrane module was simply submerged in a feed tank, in which the outer surface of the membrane was contacted with feed solution directly. In the experimental process, the feed solution was heated by a thermostatic magnetic stirring apparatus. The temperature of the feed solution was set at 75 °C throughout tests. The real-time temperature of the feed solution was measured by a temperature transmitter. The vacuum pressure of the permeate was applied to the tube side of the membrane with a water circulating multi-purpose vacuum pump. The vacuum pressure of the permeate side was controlled at −85 kPa with the deviation of ± 1.0 kPa. A condenser was installed on the permeate side to condense the water vapour and the permeate was collected in the permeate tank. The weight of permeate over the operation time was measured by an electronic balance at 30–60 min interval. The permeate quality was continuously monitored by a conductivity meter to ensure the membrane was not wetted. Permeate flux J was calculated using the Eq. (11).

$$J = \frac{m}{A \cdot t} \tag{11}$$

where, m is the weight of permeate, A is the effective area of membranes and t is the operation time.

In the case of stirring intensification S-VMDC, a magnetic rotor was placed at the bottom of the feed tank to intensify the turbulent motion of the feed, the intensification degree could be adjusted by changing the stirring rate of the magnetic rotor. For aeration intensification S-VMDC, the above magnetic rotor was replaced by a PTFE hollow fiber module acted as a simplified micro-porous air distributor unit. The detailed information was described as follows: Ten PTFE HF membranes with effective length of 25 cm were arranged in order to form a module, both sides of the module were sealed with epoxy. One side was acted as a "dead end", and the other side was acted as the access of the air. The module was then bent into a ring and fixed at the bottom of the feed

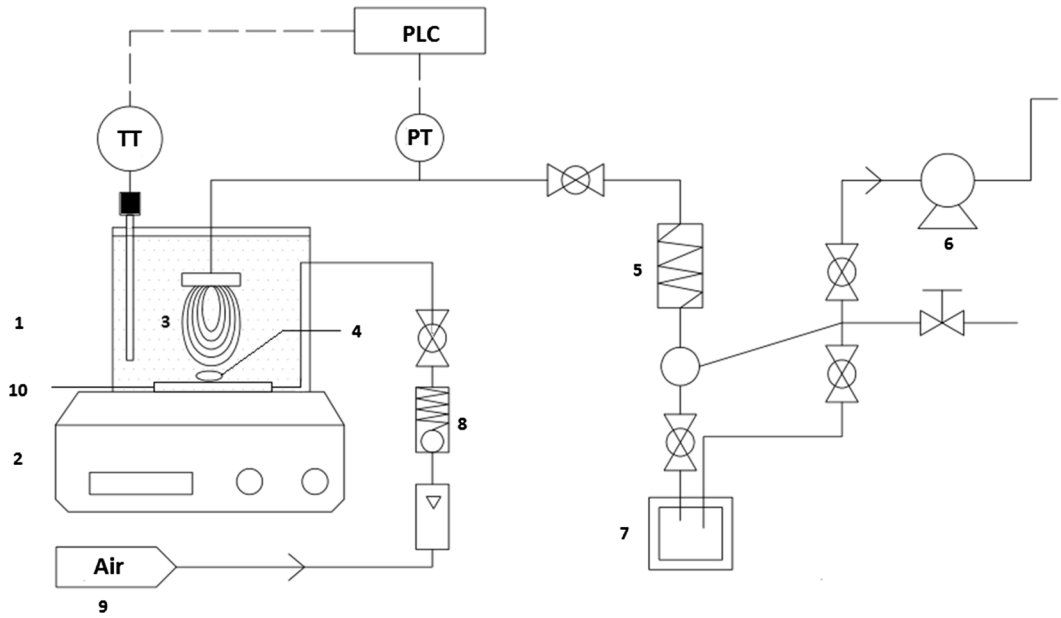

Fig. 1. Schematic of the S-VMDC setup (1) Constant temperature feed tank (Crystallizer) (2) Thermostatic magnetic stirring apparatus (3) "U-shaped " PTFE hollow fiber membrane module (4) Magnetic rotor (5) Condenser (6) Water circulating multi-purpose vacuum pump (7) Permeate tank (8) Air flow meter (9) Air compressor (10) Microporous air distributor unit *PLC: Programmable Logic Controller TT: Temperature Transmitter PT: Pressure Transmitter.

tank to provide compressed air continuously using the micro-pores of PTFE membrane. The bubble induced the turbulence of the feed to provide shear rate at the membrane surface. The pressure of compressed air was set at 0.1–0.2 MPa, the turbulent motion degree of the feed varied by adjusting the aeration rate.

Since the membrane module was reused after cleaning, the membrane performance showed small difference in each experiment. As a result, prior to each experiment, the pure water flux J_0 was measured with deionized (DI) water as feed over 1 h at the operating temperature of 75 °C and vacuum pressure of -85 KPa without any turbulent intensification mode. The flux data in all concentration experiments were presented in terms of normalized flux ratio J/J_0 [40] in order to make intuitive comparison. The concentration level was express in terms of volume concentration factor (VCF), which is defined as a ratio of initial feed volume to concentration volume [12]. The critical VCF in this experiment is defined as the volume concentration factor at which the normalized flux began to drop significantly in a short period of time. The duration of the experiment was depended on the permeate flux reduction. When the value of J/J_0 decreased below 0.2, the experiment was terminated.

At the completion of the concentration process, the membrane module was taken out from the feed tank and immediately immersed in a certain volume of DI water. In this process, NaCl crystals on the membrane surface completely dissolved in DI water. The weight of NaCl crystals on the membrane surface could be calculated according to the measured value of the total dissolve solid (TDS) and the volume of the immersion solution. The bulk solution was cooled to room temperature by natural cooling, filtered by a filter paper and then dried in a 100 °C oven to constant weight. The weight of NaCl crystals harvested in bulk solution was measured by an electronic balance. In order to achieve zero liquid discharge, a volume of 250–300 mL residue solution was reheated to 100 °C by the constant temperature magnetic stirrer, and the stirring rate was kept at 300 rpm to accelerate the evaporation process. When a large amount of NaCl crystals were separated out by evaporation, the heating equipment was turned off and a small amount of water was removed by waste heat. The NaCl crystals were also dried in 100 °C oven to constant weight to make sure that all the water had been removed. The weight of NaCl crystals collected by evaporation was also measured by the electronic balance to make material balance.

3.5. Crystal size distribution (CSD)

The particle size distribution of NaCl crystals harvested in bulk solution were measured using a Mastersizer 2000 with the size range from 0.02 to 2000 μm. Crystal samples were dispersed in ethanol by ultrasonic dispersion. Triplicate measurements were conducted for each sample.

4. Results and discussion

4.1. Performance of S-VMDC for concentrating NaCl solution

The S-VMDC test was firstly executed for concentrating 100 g/L NaCl solution in stagnant feed solution. The normalized flux and permeate conductivity were monitored continuously and the result was shown as a function of VCF. As illustrated in Fig. 2, a gradually decrease of the normalized flux was observed with the VCF increased up to a critical level, at which point a rapid flux decline occurred. The gradual flux decline before the occurrence of the critical VCF was principally

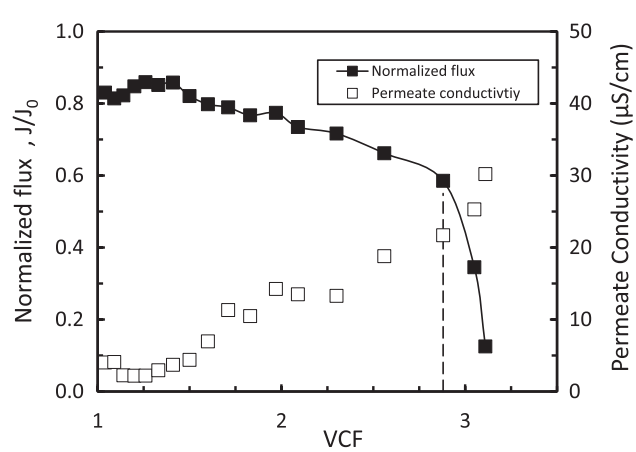

Fig. 2. Normalized flux and permeate conductivity as a function of VCF for concentrating 100 g/L NaCl solution. The pure water flux J_0 was 6.23 kg/m^2 h. Feed temperature 75 °C; Vacuum pressure −85 KPa.

Fig. 3. NaCl crystals formed (A) on the membrane surface and (B) in the bulk solution.

owing to the depression of vapour pressure caused by the increase of feed concentration. Once the VCF exceeded the critical VCF value, drastic flux decline was observed due to the combined effect of surface and bulk crystallization [12].

It is known that supersaturated solutions exhibit a metastable zone, which constitutes the allowable supersaturation level [41]. Spontaneous nucleation occurs only when a certain degree of supersaturation is reached, which is known as the metastable limit. Considering that there were no presence of any crystallize matters in the original feed solution in this experiment, the initial mechanism of nucleation was the primary nucleation. The primary nucleation can be subdivided into the homogeneous nucleation in the bulk solution and heterogeneous nucleation on the membrane surface [41]. In the absence of turbulent intensification, the latter played a more dominated role since the microporous membrane usually acted as a promoter of heterogeneous nucleation [42,43]. Along with the effect of temperature and concentration polarization, the feed concentration on membrane surface could easily exceed the meatastable limit of NaCl solution, which lead to the formation and growth of crystals preferentially occurred on the membrane surface. As it was shown in Fig. 3(A), large numbers of needle-shaped crystals with nonuniform size partially covered the membrane surface, reducing the open pore area available for water to vaporize. It was the main reason for flux attenuation beyond the critical VCF [44]. As shown in Fig. 3(B), some crystals were also formed in the bulk solution, the size of them were nonuniform as well.

The start of surface crystallization can be identified by the occurrence of the critical VCF and that of bulk crystallization can be observed with naked eyes by the sudden increase of turbidity in the feed solution. In the case of S-VMDC test in stationary feed, sudden crystallization event was observed at VCF of approximately 3.05, preceded by the occurrence of surface crystallization at the critical VFC of 2.88. This was the evidence that the crystallization behavior was dominated by the heterogeneous nucleation and crystal growth on the membrane surface in the S-VMDC process.

The initial permeate conductivity maintained below 10 μS/cm, indicating the high rejection factor achieved by S-VMDC. Although the conductivity of the permeate showed growing tendency with the increase of VCF due to the crystallization fouling [10], it still maintained below 30 μS/cm at the end of the experiment, which confirmed that the membrane pores did not suffer from severe wetting.

4.2. Stirring intensification S-VMDC for concentrating NaCl solution

4.2.1. Effect of stirring rate on S-VMDC performance

The S-VMDC performance at various stirring rates was investigated and the result was compared with that in stationary feed. The normalized flux and permeate conductivity as a function of VCF was illustrated in Fig. 4. The corresponding critical and final VCF were listed in Table 2. In the case of S-VMDC in stationary NaCl solution, the initial flux was 15–20% lower than pure water flux at the same experimental

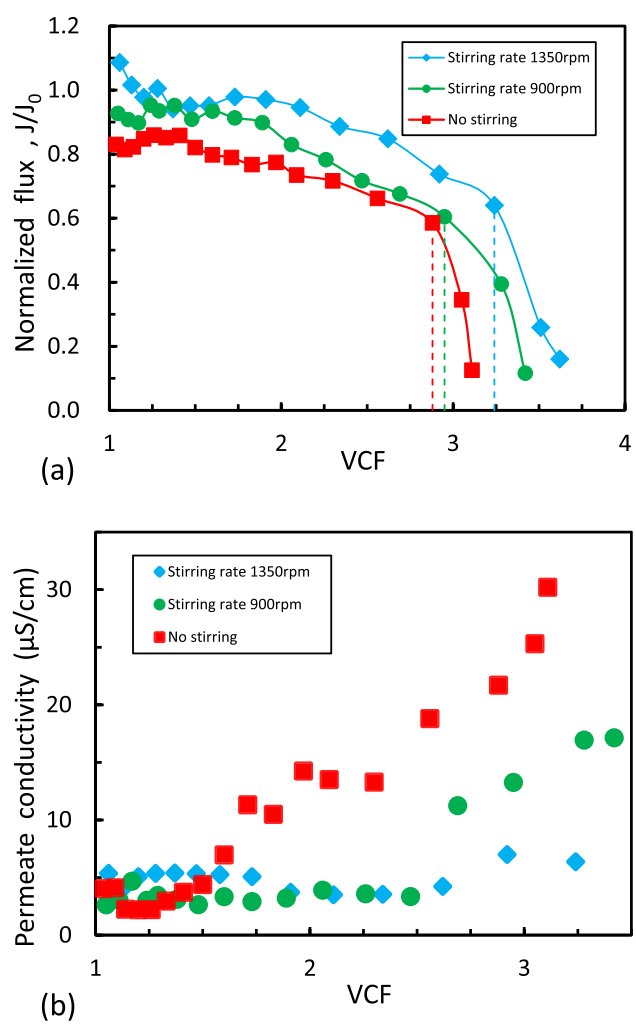

Fig. 4. Effect of stirring rate on S-VMDC performance for concentrating 100 g/L NaCl solution. (a) Normalized flux and (b) Permeate conductivity as a function of VCF. Feed temperature 75 °C; Vacuum pressure −85 KPa. J_0 was 6.51 ± 0.20 kg/m^2 h.

Table 2
The critical and final VCF in S-VMDC for concentrating NaCl solution at various stirring rates.

Stirring rate (rpm)	0	900	1350
$VCF_{critical}$	2.88	2.95	3.24
VCF_{final}	3.11	3.42	3.62

condition due to the vapour pressure depression and polarization phenomenon. Apparently better performance was achieved with stirring intensification S-VMDC. The effect of temperature polarization was weakened with the help of stirring intensification, which signified that the temperature on the membrane surface were closer to that in the bulk solution. Flux decline due to the vapor pressure depression was compensated by the increase of temperature on the membrane surface in the initial stage. Therefore, the initial flux was closed to or even a little higher than that of pure water without stirring. In addition, the increase of turbulent degree of feed solution also reduced the chances of heterogeneous nucleation on the membrane surface. It was suggested that homogeneous nucleation in the bulk solution played a more dominated role gradually. It could be observed that some tiny crystals had already formed in the bulk solution before the occurrence of flux attenuation, which confirmed the above suggestion. The combination of all above factors will have impact on the metastable zone of NaCl solution [41], making it more difficult for the concentration on the membrane surface and in the bulk solution surpassed the metastable limit. As a result, the critical VCF increased from 2.88 to 3.24 when the stirring rate increased from 0 to 1350 rpm. In terms of the permeate quality, it was found that the permeate conductivity maintained at lower level with higher stirring rate (Fig. 4b), which indicated the lower tendency of partial wetting with the decrease of salt crystals on the membrane surface.

4.2.2. Effect of stirring rate on NaCl crystallization

In order to further investigate the effect of stirring intensification on crystallization behavior in this process, the weight of NaCl crystals produced on membrane surface and in bulk solution at different experimental conditions were compared, as shown in Fig. 5. The material balance in this process was also calculated and the deviation was less than 3% (Table 3). It was obvious that NaCl crystals produced on the membrane surface decreased with increasing stirring rate. Oppositely, NaCl crystals produced in bulk solution significantly increased with the

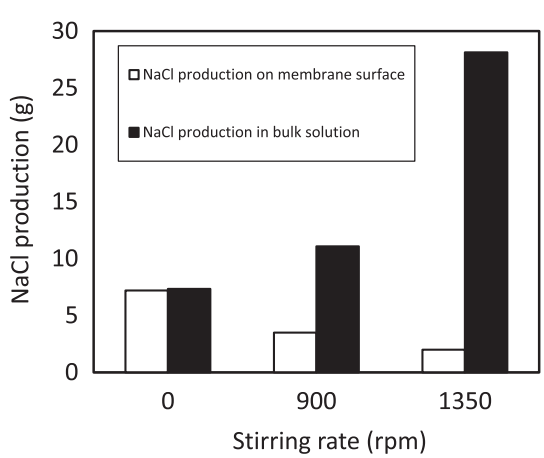

Fig. 5. The weight of NaCl production in S-VMDC process at various stirring rates. Feed temperature 75 °C; Vacuum pressure −85 KPa.

Table 3
The weight of NaCl production on membrane surface, in bulk solution and by residual solution evaporation at various stirring rates.

Stirring rate (rpm)	The weight of NaCl production (g)			
	On membrane surface	In bulk solution	By residual solution evaporation	Total
0	7.2	7.34	82.58	97.12
900	3.5	11.08	83.37	97.95
1350	2.0	28.13	68.88	99.01

increase of stirring rate. Although the heterogeneous nucleation and crystal growth on the membrane surface were still possible, the crystals were more inclined to nucleate in bulk solution due to the improvement of turbulent degree. In addition, the shear force provided by stirring increased the chances of collision between crystals, which promoted the secondary nucleation in the bulk solution. It was indicated that the primary crystallization behavior after the occurrence of the critical VCF gradually converted from crystal growth on the membrane surface to the secondary nucleation in the bulk solution with the help of stirring intensification.

Fig. 6 presented the effect of stirring rate on crystal size distribution (CSD) of NaCl produced in bulk solution. The mean crystal size was also listed in Table 4. It can be seen that the peak value of CSD moved slightly to the left side and the volume weighted mean D[4,3] decreased from 482.4 to 428.7 μm when the stirring rate increased from 900 to 1350 rpm. Since there is competitive relationship between the crystal nucleation and growth [18], the increase of chances for secondary nucleation at higher stirring rate limited the growth of the crystals. As a result, the formation of large-sized crystals was suppressed and the average crystal size became smaller.

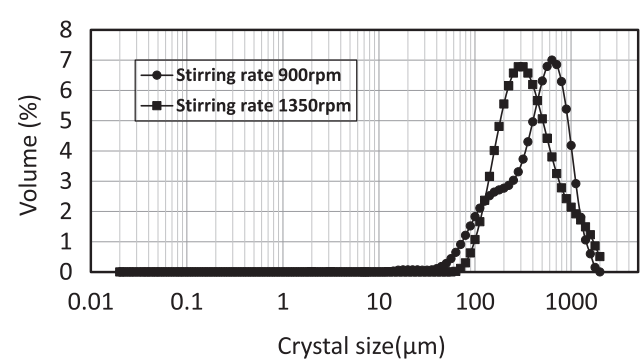

Fig. 6. Crystal size distribution (CSD) of NaCl produced in bulk solution at various stirring rates.

Table 4
The crystal size produced in bulk solution at various agitation modes.

Agitation mode	d (0.5) (μm)	D[4,3] (μm)
Stirring (rpm)		
900	442.1	482.4
1350	317.1	428.7
Aeration (m^3/h)		
0.16	389.4	431.5
0.20	305.7	381.0

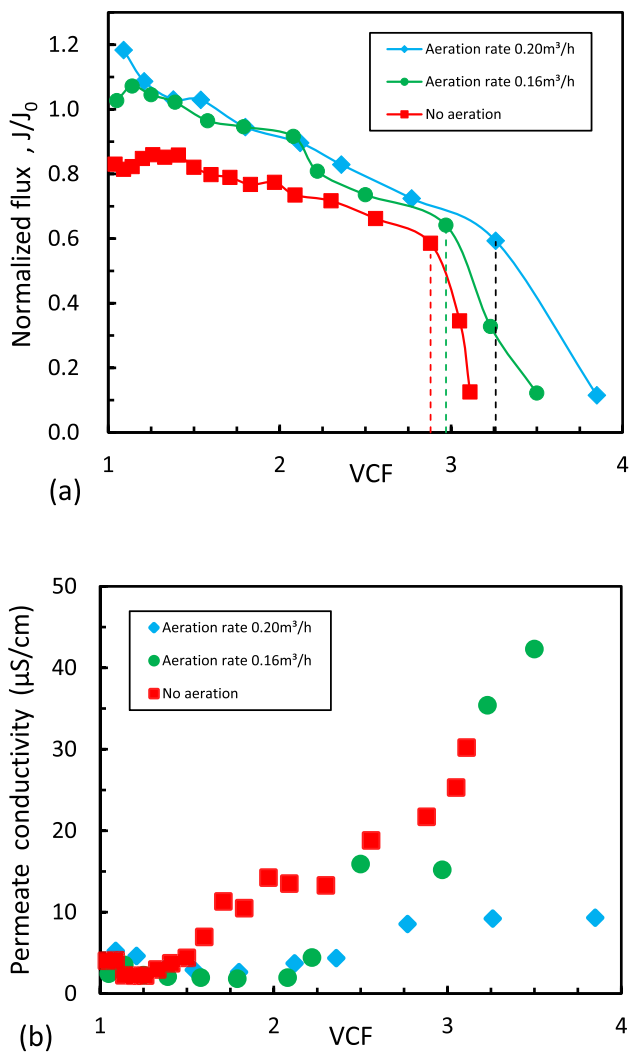

Fig. 7. Effect of aeration rate on S-VMDC performance for concentrating 100 g/L NaCl solution. (a) Normalized flux and (b) Permeate conductivity as a function of VCF. Feed temperature 75 °C; Vacuum pressure −85 KPa. J_0 was 6.33 ± 0.11 kg/m^2 h.

4.3. Aeration intensification S-VMDC for concentrating NaCl solution

4.3.1. Effect of aeration rate on S-VMDC performance

Aeration was applied as another turbulent intensification method to improve the S-VMDC performance. The detailed information about micro-porous air distributor unit was shown in Section 3.4. The advantage of this approach was that it could control the initial size of air bubbles at the micron level. In addition, it was beneficial to achieve denser and more uniform distribution of air-bubbles. The normalized flux and permeate conductivity as a function of VCF was illustrated in Fig. 7. The critical and final VCF were shown as Table 5. Similar to the stirring intensification S-VMDC process, higher permeate flux and critical VCF could be also obtained with the help of aeration under the same experimental condition. With the gas-liquid two-phase flow, the turbulent extent of membrane surface and bulk solution increased effectively, leading to the decrease of both temperature and concentration polarization, which improved the permeate flux. But it was presented that when aeration rate maintained constant, the positive effect of aeration intensification on the permeate flux was weakened with the increase of VCF. It was probably due to the fact that the negative influence of feed concentration on permeate flux was more prominent with higher VCF, making the effect of aeration intensification less obvious.

Table 5
The critical and final VCF in S-VMDC for concentrating NaCl solution at various aeration rates.

Aeration rate (m^3/h)	0	1.6	2.0
$VCF_{critical}$	2.88	2.97	3.26
VCF_{final}	3.11	3.50	3.85

Moreover, when further increased the aeration rate from 0.16 to 0.20 m^3/h, the permeate flux did not make further significant improvement. Although further increasing the aeration rate was conducive to promote the heat and mass transfer, air-bubbles produced by higher aeration rate could easily adhere to the membrane surface, reducing the effective evaporation area which prevented the further improvement of permeate flux. However, the existence of air-bubbles on the membrane surface reduced the chances of membrane surface crystallization and the likelihood of salt crystals penetrate into the membrane pores. As a result, the permeate conductivity maintained at a relatively low level throughout the experiment when aeration rate was 0.20 m^3/h. On the other hand, as it was shown in Table 5, the critical VCF increased obviously with the increase of aeration rate from 0.16 to 0.20 m^3/h. It probably signified that the aeration rate of 0.16 m^3/h was large enough to improve the permeate flux, but was not large enough to increase the metastable limit of NaCl solution.

It was worth noting that the introduction and departure of air-bubbles inevitably took away some of the heat, consequently, the heating power must be increased in order to keep the temperature in feed solution constant. Therefore, the additional energy consumption should be fully considered for the actual application.

4.3.2. Effect of aeration rate on NaCl crystallization

As shown in Fig. 8 and Table 6, the S-VMDC process with aeration rate of 0.20 m^3/h harvested the highest number of NaCl crystals in bulk solution at the end of the experiment, which was much higher than that of produced without aeration. The significant increase of NaCl production in the bulk solution was mainly due to the increase of the critical and final VCF, which indicated the transformation of the crystallization mechanism. Julian et al. [17] also reported that aeration could promote additional nucleation of crystals in the bulk feed and reduced the opportunity of salts precipitation on the membrane surface.

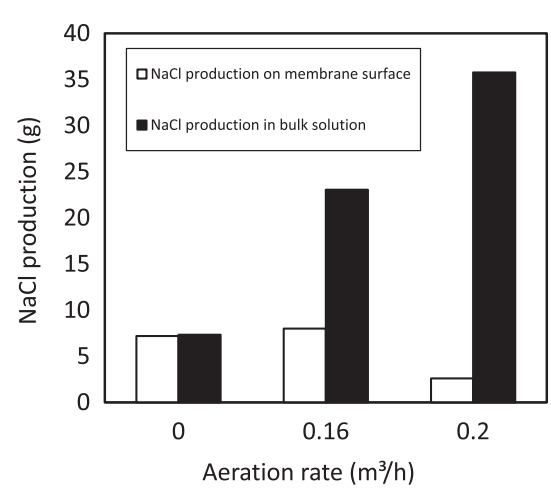

Fig. 8. The weight of NaCl production of S-VMDC operation at various aeration rates. Feed temperature 75 °C; Vacuum pressure −85 KPa.

Table 6
The weight of NaCl production on membrane surface, in bulk solution and by residual solution evaporation at various aeration rates.

Aeration rate (m^3/h)	The weight of NaCl production (g)			
	On membrane surface	In bulk solution	By residual solution evaporation	Total
0	7.20	7.34	82.58	97.12
0.16	8.00	23.05	65.91	96.96
0.20	2.60	35.76	60.05	98.41

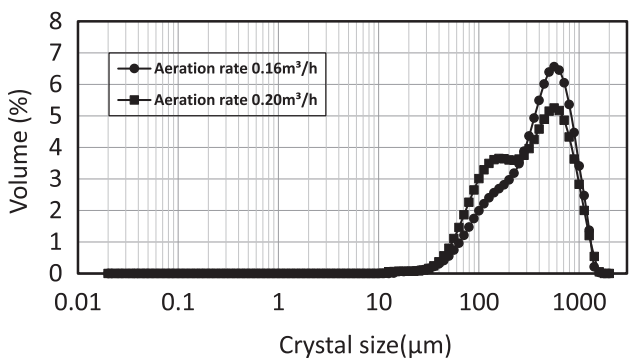

Fig. 9. Crystal size distribution (CSD) of NaCl produced in bulk solution at various aeration rates.

The experimental result in this study at aeration rate of 0.20 m^3/h confirmed this conclusion. However, when the aeration rate decreased to 0.16 m^3/h, crystals deposited on membrane surface did not decrease although bulk crystallization was still promoted. It probably suggested that the aeration rate of 0.16 m^3/h was not large enough to inhibit surface crystallization in this experiment.

The effect of aeration rate on the mean crystal size and CSD of NaCl produced in the bulk solution was shown in Table 4 and Fig. 9, respectively. In the case of aeration rate at 0.16 m^3/h, the CSD reached its peak value at about 632 μm. When the aeration rate increased to 0.20 m^3/h, the main peak remained unchanged with lower volume percentage and another peak appeared around 200 μm. It indicated that the intensive-mixing cased by higher aeration rate make a rapid increase of the shear force, easily leading to the breakage of the particles. Therefore, a number of crystals will smaller size formed under this experiment condition and the volume weighted mean D[4,3] decreased from 389.4 to 305.7 μm when the aeration rate increased from 0.16 to 0.20 m^3/h. Moreover, due to the formation of smaller-sized crystals, the value of span and uniformity of CSD increased to 2.36 and 0.75 respectively, larger than that of 1.89 and 0.59 with the aeration rate of 0.16 m^3/h, which signified that the CSD turned wider and the uniformity decreased with intensive aeration.

4.4. Performance of integrated stirring and aeration intensification S-VMDC for concentrating NaCl solution

The combined effect of stirring and aeration intensification on the performance of S-VMDC was also investigated and results were shown in Figs. 10 and 11 and Table 7. A stirring rate of 1350 rpm and aeration rate of 0.20 m^3/h were applied. Comparing with turbulent intensification in a single mode, the permeate flux increased slightly but not significantly before the sudden crystallization occurred in this test. The

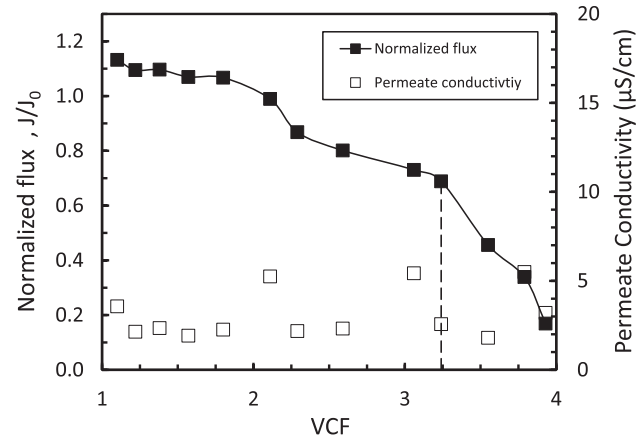

Fig. 10. Normalized flux and permeate conductivity as a function of VCF for concentrating 100 g/L NaCl solution. The pure water flux J_0 was 6.27 kg/m^2 h. Feed temperature 75 °C; Vacuum pressure −85 KPa. Stirring rate of 1350 rpm and aeration rate of 0.20 m^3/h.

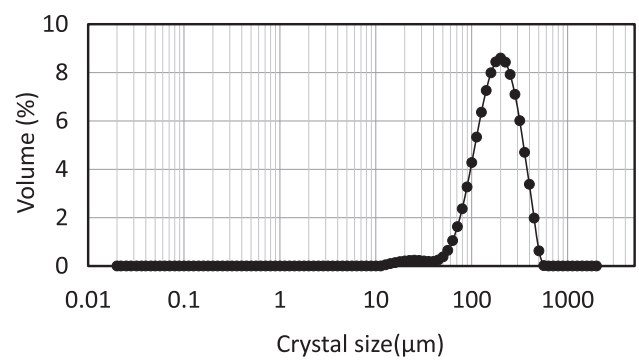

Fig. 11. Crystal size distribution (CSD) of NaCl produced in bulk solution. Feed temperature 75 °C; Vacuum pressure −85 KPa. Stirring rate of 1350 rpm and aeration rate of 0.20 m^3/h.

Table 7
The combined effect of stirring and aeration intensification on the performance of S-VMDC.

Performance of S-VMDC for concentrating NaCl solution		
VCF $_{critical}$		3.24
VCF $_{final}$		3.93
Performance of NaCl crystallization		
The weight of NaCl production (g)	On the membrane surface	2.53
	In bulk solution	31.85
	By residual solution evaporation	62.68
Crystal size in bulk solution (μm)	d(0.5)	175.3
	D[4,3]	190.4

critical VCF kept almost unchanged which suggested that further improved the degree of mixing of bulk solution could not continue to increase the metastable limit [45] of NaCl solution. The combined effect of stirring and aeration mainly reflected in two aspects. Firstly, the flux attenuation rate after the critical VCF obviously slowed down (Fig. 10). It probably owed to the synergy effect of shear force provided by stirring and aeration, which further decreased the rate of growth and deposition of crystals on the membrane surface. Secondly, the size

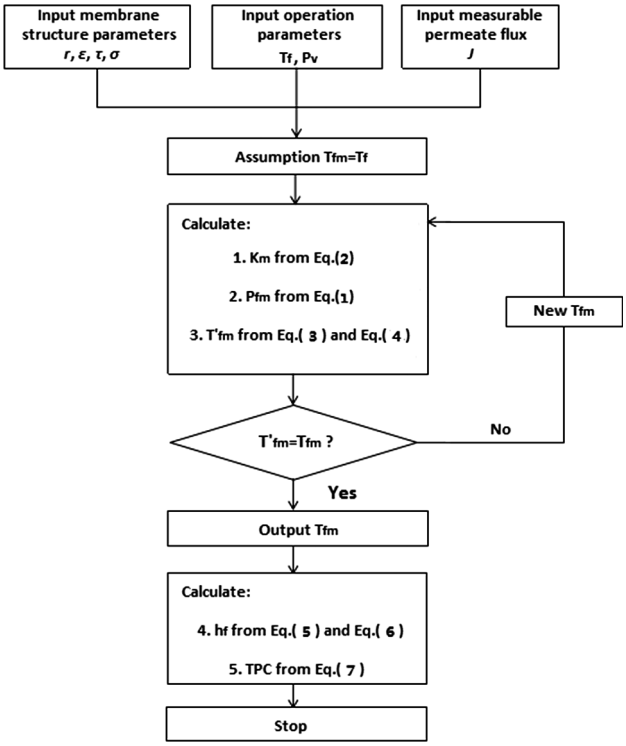

Fig. 12. A VMD model algorithm.

distribution of crystallized product was relatively narrow and crystal size became much smaller with the help of combined effect of stirring and aeration (Fig. 11). As might be expected, larger-sized crystals were limited and the formation of smaller-sized crystals were promoted. The change of crystal size and distribution with various turbulent intensification modes means that the ideal crystallized product can be obtained by selecting an optimal turbulent intensification condition.

4.5. Analysis of heat transfer under different turbulent intensification modes

In order to quantitative analyze the effect of turbulent intensification on heat transfer in S-VMDC process, the variation of h_f and TPC before the occurrence of critical VCF under different agitation modes in this test were calculated according to the theory described in Section 2. To derive the values of both h_f and TPC, the value of T_{fm} is necessary. But it is worth noting that the value of T_{fm} cannot be measured directly due to the presence of the feed boundary layer. As a result, T_{fm} is derived by means of an iterative method from Eq.(1)–(4), as shown in Fig. 12. Firstly, assuming the value of T_{fm} was equal to that of T_f to obtain a first value of K_m from Eq. (2). Secondly, the obtained value of K_m was used to get the value of P_{fm} from Eq. (1). Finally, according to the combination of Eq. (3) and Eq. (4), a new value of T_{fm} was obtained. This process was repeated several times until an invariant value of T_{fm} was reached. Then the value of h_f and TPC was calculated from Eq. (5)–(7).

The results were shown as Fig. 13. In the case of SVMD in stationary feed (Fig. 13 a-1 [1]marked in red), the heat transfer was dominated by free convection, thus the value of h_f was small and was little affected by the increase of VCF. According to the calculation results, the descent degree of permeate flux with the increase of VCF was basically in line with that of vapour pressure depression with VCF, which indicated the flux decline was totally attribute to the vapour pressure depression caused by the increase of feed concentration. The reduction of driving force due to the increase of feed concentration was compensated by the increase of membrane surface temperature, which lead to the decrease of temperature polarization at higher VCF.

When focused on the SVMD with stirring intensification (Fig. 13a-1 marked in green and blue), the dominating heat transfer method gradually converted from free convection to forced convection with the help of stirring intensification. As a result, the heat transfer condition in boundary layer was improved and h_f increased with the increase of stirring rate since higher Reynolds numbers could be achieved with higher stirring rate. When the stirring rate remained constant, it was interesting to note that the value of h_f showed a downward trend with the increase of VCF. It probably due to the fact that the viscosity and density of the feed solution significantly increased at higher VCF, which weakened the strengthening effect of stirring on heat transfer in boundary.

When focused on the SVMD with aeration intensification, a similar law was shown in the case of aeration intensification (Fig. 12b-1), indicating that the heat transfer condition in boundary layer could also be improved with the help of aeration intensification. When the aeration rate kept constant, the value of h_f also presented downtrend with the increase of VCF, especially when the aeration rate increased to 0.20 m^3/h. In the aeration intensification mode, the gas-liquid flow was relatively evenly distributed in feed tank, as a result, the influence of feed volume on the mixing degree was less obvious. But the ratio of gas-liquid increased significantly with the increase of VCF even at the same aeration rate, which influenced the heat transfer effect.

As it was shown in Fig. 13a-2 and b-2, the value of TPC increased with the help of both stirring and aeration intensification, which indicated that both stirring and aeration intensification were conducive to reduce the heat transfer resistance and the process was more likely to be mass transfer controlled at higher concentration. It should also be pointed out that although the heat transfer effect could be improved by the introduction of stirring and aeration, the increase of Reynolds number was still limited under the existing operation conditions. As a consequence, the mass transfer coefficient in submerged MD system in our experiment was still relatively small comparing with that in conventional cross-flow MD system which were reported in previous papers [8,46]

5. Conclusion

This study demonstrated that the integration of MD and crystallization was achievable by exploring a lab-scale S-VMDC system. Pure water with reasonable permeate flux and crystallized products with desirable size distribution could be produced simultaneously when concentrated highly concentration NaCl solution. The influence of both stirring and aeration intensification on the MD performance and crystallization behavior was mainly manifested in the following conclusions:

1. Both stirring and aeration were conducive to improve the heat transfer in boundary layer and weaken the polarization phenomenon, thus increasing the MD performance. The improvement effect was more pronounced with the increase of stirring or aeration intensity.

2. The dominated crystallization behavior converted from surface crystallization to bulk crystallization with the help of both stirring and aeration intensification, leading to the increase of the critical VCF. As a consequence, the MD process could operate under a higher supersaturated condition and the production of NaCl crystals increased significantly.

3. The size and size distribution of crystallized product could be regulated and controlled by selecting an optimal turbulent intensification mode. Larger-sized crystals were limited and the formation of smaller crystals were promoted with the help of combined effect of stirring at 1350 rpm and aeration at 0.20 m^3/h.

[1] For interpretation of color in Fig. 13, the reader is referred to the web version of this article.

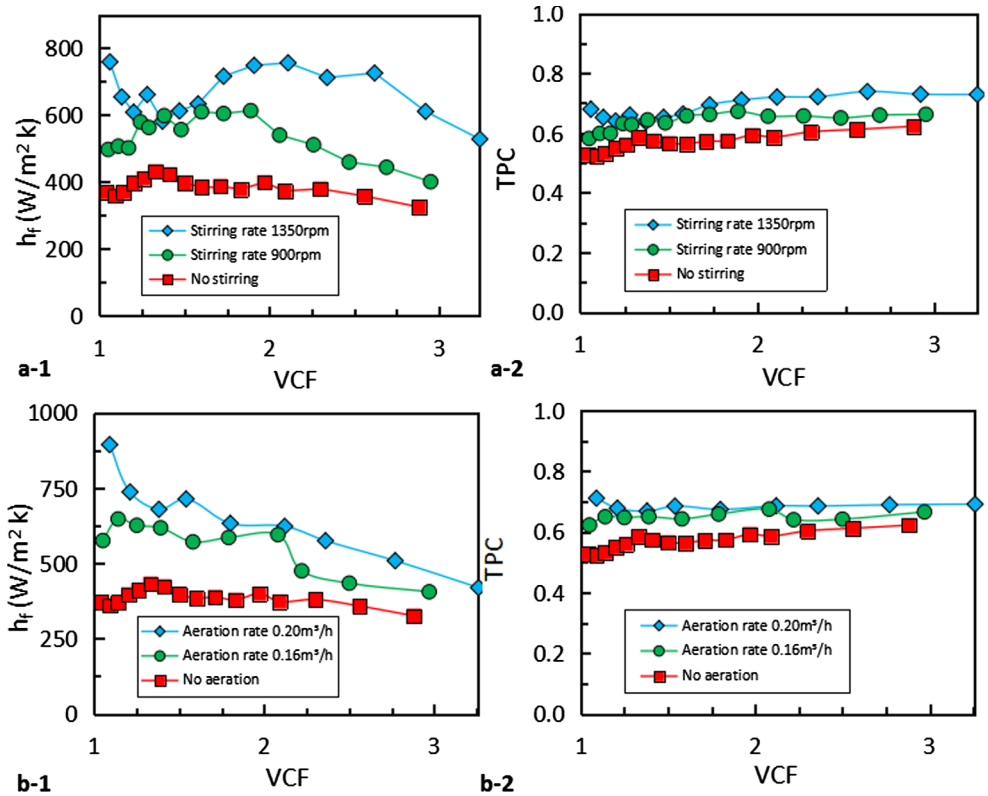

Fig. 13. The variation of h_f and TPC as a function of VCF under different turbulent intensification modes.

Acknowledgment

All the authors thank the financial support from Youth Innovation Promotion Association of the Chinese Academy of Sciences (No. 2016171).

Appendix A. Supplementary material

Supplementary data to this article can be found online at https://doi.org/10.1016/j.seppur.2018.09.072.

References

[1] M. Khayet, Membranes and theoretical modeling of membrane distillation: a review, Adv. Colloid Interface Sci. 164 (1–2) (2011) 56.
[2] C. Liu, A.R. Martin, The use of membrane distillation in production for the semiconductor industry, Crop Res. (2014).
[3] F. Edwie, T.S. Chung, Development of hollow fiber membranes for water and salt recovery from highly concentrated brine via direct contact membrane distillation and crystallization, J. Membr. Sci. 421–422 (12) (2012) 111–123.
[4] J.P. Mericq, S. Laborie, C. Cabassud, Vacuum membrane distillation of seawater reverse osmosis brines, Water Res. 44 (18) (2010) 5260–5273.
[5] Y. Yun, et al., Direct contact membrane distillation mechanism for high concentration NaCl solutions, Desalination 188 (1) (2006) 251–262.
[6] G. Chen, et al., Optimization of operating conditions for a continuous membrane distillation crystallization process with zero salty water discharge, J. Membr. Sci. 450 (2014) 1–11.
[7] X. Jiang, et al., Progress in membrane distillation crystallization: process models, crystallization control and innovative applications, Front. Chem. Sci. Eng. (2017) 1–16.
[8] F. Edwie, T.S. Chung, Development of simultaneous membrane distillation–crystallization (SMDC) technology for treatment of saturated brine, Chem. Eng. Sci. 98 (29) (2013) 160–172.
[9] M.T. Chan, et al., Membrane distillation crystallization of concentrated salts—flux and crystal formation, J. Membr. Sci. 257 (1) (2005) 144–155.
[10] J.A. Sanmartino, et al., Desalination and concentration of saline aqueous solutions up to supersaturation by air gap membrane distillation and crystallization fouling, Desalination 393 (2016) 39–51.
[11] R. Creusen, et al., Integrated membrane distillation–crystallization: process design and cost estimations for seawater treatment and fluxes of single salt solutions, Desalination 323 (16) (2013) 8–16.
[12] Y. Shin, J. Sohn, Mechanisms for scale formation in simultaneous membrane distillation crystallization: effect of flow rate, J. Ind. Eng. Chem. 35 (2016) 318–324.
[13] G. Chen, et al., Performance enhancement and scaling control with gas bubbling in direct contact membrane distillation, Desalination 308 (1) (2013) 47–55.
[14] G. Chen, et al., Heat transfer intensification and scaling mitigation in bubbling-enhanced membrane distillation for brine concentration, J. Membr. Sci. 470 (6) (2014) 60–69.
[15] C. Wu, et al., Study on the heat and mass transfer in air-bubbling enhanced vacuum membrane distillation, Desalination 373 (5) (2015) 16–26.
[16] M.M. Teoh, S. Bonyadi, T.S. Chung, Investigation of different hollow fiber module designs for flux enhancement in the membrane distillation process, J. Membr. Sci. 311 (1–2) (2008) 371–379.
[17] H. Julian, et al., Effect of operation parameters on the mass transfer and fouling in submerged vacuum membrane distillation crystallization (VMDC) for inland brine water treatment, J. Membr. Sci. 520 (2016) 679–692.
[18] G.N. Youngkwon Choi, Sanghyun Jeong, Saravanamuthu Vigneswaran, Sangho Lee, Rong Wang, Anthony G. Fane, Experimental comparison of submerged membrane distillation configurations for concentrated brine treatment, Desalination 420 (2017) 54–62.
[19] S. Meng, et al., Submerged membrane distillation for inland desalination applications, Desalination 361 (2015) 72–80.
[20] H. Julian, et al., Scaling mitigation in submerged vacuum membrane distillation and crystallization (VMDC) with periodic air-backwash, J. Membr. Sci. (2017).
[21] T. Zou, et al., Fouling behavior and scaling mitigation strategy of $CaSO_4$ in submerged vacuum membrane distillation, Desalination 425 (2018) 86–93.
[22] W. Zhong, et al., Fouling mitigation in submerged VMD for the treatment of brackish groundwater concentrates with transverse vibration and crystallizer, Desalination 426 (2017) 32–41.
[23] A.S. Alsaadi, et al., Experimental and theoretical analyses of temperature polarization effect in vacuum membrane distillation, J. Membr. Sci. 471 (6) (2014) 138–148.
[24] M. Qtaishat, et al., Heat and mass transfer analysis in direct contact membrane distillation, Desalination 219 (1–3) (2008) 272–292.
[25] J.I. Mengual, M. Khayet, M.P. Godino, Heat and mass transfer in vacuum membrane distillation, Int. J. Heat Mass Transf. 47 (4) (2004) 865–875.
[26] R.W. Schofield, A.G. Fane, C.J.D. Fell, Heat and mass transfer in membrane distillation, J. Membr. Sci. 33 (3) (1987) 299–313.
[27] S.G. Lovineh, M. Asghari, B. Rajaei, Numerical simulation and theoretical study on simultaneous effects of operating parameters in vacuum membrane distillation, Desalination 314 (8) (2013) 59–66.
[28] M. Khayet, T. Matsuura, Pervaporation and vacuum membrane distillation processes: modeling and experiments, Aiche J. 50 (8) (2004) 1697–1712.
[29] C.K. Chiam, R. Sarbatly, Vacuum membrane distillation processes for aqueous solution treatment—a review, Chem. Eng. Process. Process Intensif. 74 (8) (2013) 27–54.

[30] H. Zhu, et al., Preparation and properties of PTFE hollow fiber membranes for desalination through vacuum membrane distillation, J. Membr. Sci. 446 (1) (2013) 145–153.
[31] E. Drioli, A. Ali, F. Macedonio, Membrane distillation: recent developments and perspectives, Desalination 356 (2015) 56–84.
[32] H.J. Hwang, et al., Direct contact membrane distillation (DCMD): experimental study on the commercial PTFE membrane and modeling, J. Membr. Sci. 371 (1–2) (2011) 90–98.
[33] S. Adnan, et al., Commercial PTFE membranes for membrane distillation application: effect of microstructure and support material, Desalination 284 (2) (2012) 297–308.
[34] J. Jia, G. Kang, Y. Cao, Effect of stretching parameters on structure and properties of polytetrafluoroethylene hollow-fiber membranes, Chem. Eng. Technol. 39 (5) (2016) 935–944.
[35] J. Jia, et al., Sintering process investigation during polytetrafluoroethylene hollow fibre membrane fabrication by extrusion method, High Perform. Polym. 29 (1) (2017) 095400831666940.
[36] X. Jian, Z.L. Xu, Poly(vinyl chloride) (PVC) hollow fiber ultrafiltration membranes prepared from PVC/additives/solvent, J. Membr. Sci. 208 (1) (2002) 203–212.
[37] H. Yasuda, J.T. Tsai, Pore size of microporous polymer membranes, J. Appl. Polym. Sci. 18 (3) (2010) 805–819.
[38] J.A. Otero, et al., Three independent ways to obtain information on pore size distributions of nanofiltration membranes, J. Membr. Sci. 309 (1) (2008) 17–27.
[39] M.C. García-Payo, M. Essalhi, M. Khayet, Effects of PVDF-HFP concentration on membrane distillation performance and structural morphology of hollow fiber membranes, J. Membr. Sci. 347 (1–2) (2010) 209–219.
[40] S. Srisurichan, R. Jiraratananon, A.G. Fane, Humic acid fouling in the membrane distillation process, Desalination 174 (1) (2005) 63–72.
[41] J. Ulrich, C. Strege, Some aspects of the importance of metastable zone width and nucleation in industrial crystallizers, J. Cryst. Growth 237–239 (3) (2002) 2130–2135.
[42] X. Ji, et al., Membrane distillation-crystallization of seawater reverse osmosis brines, Sep. Purif. Technol. 71 (1) (2010) 76–82.
[43] X. Jiang, et al., A novel membrane distillation response technology for nucleation detection, metastable zone width measurement and analysis, Chem. Eng. Sci. 134 (2015) 671–680.
[44] M. Ramezanianpour, M. Sivakumar, An analytical flux decline model for membrane distillation, Desalination 345 (345) (2014) 1–12.
[45] K.K. Chaitanya, D. Sarkar, Determination of the metastable zone width by a simple optical probe, Chem. Eng. Technol. 37 (6) (2014) 1037–1042.
[46] S. Meng, et al., Crystallization behavior of salts during membrane distillation with hydrophobic and superhydrophobic capillary membranes, J. Membr. Sci. 473 (2015) 165–176.